# Effect of Composite Fabrication Method on Structural Response and Impact Damage

Dawn C. Jegley*
*NASA Langley Research Center, Hampton, Virginia 23665*
and
Osvaldo F. Lopez†
*Federal Aviation Administration, Atlanta, Georgia 30349*

**Experimentally determined axial compressive failure loads, strains, and failure modes of composite flat panels and cylinders are presented. A comparison of two types of filament-wound flat graphite-epoxy panels indicates that the winding pattern can influence structural response. A comparison of hand laid-up tape and filament-wound composite cylinders indicates that fabrication method may not significantly influence the failure mode or average failure strain of thick-walled (radius-to-thickness ratio less than 15) graphite-epoxy cylinders. The interaction of manufacturing-induced features (fiber crossovers) and low-speed impact damage for graphite-epoxy specimens is also presented. Filament-wound flat panels with many fiber crossovers exhibited lower failure strains than did filament-wound panels without fiber crossovers for all impact speeds examined. Graphite-thermoplastic cylinders exhibited a significantly different failure mode from graphite-epoxy cylinders.**

## Introduction

COMPOSITE materials can be used to construct lightweight, structurally efficient components for aircraft applications. Graphite-epoxy and graphite-thermoplastic parts can be used to replace many aluminum parts on today's aircraft. However, the low density and high stiffness and strength of laminated composites do not necessarily make them practical alternatives to metals for all applications, since composites exhibit different failure mechanisms, properties, etc., from metals. Fabrication techniques used to construct composite parts differ from those used to construct metallic parts. Until recently, most graphite-epoxy parts were fabricated from unidirectional tape using an expensive and labor-intensive hand lay-up procedure. Other methods of construction, such as filament winding, could significantly reduce the cost of fabrication and may improve the quality of some structures. However, few studies of the effects on structural response of fabrication-induced features, such as fiber crossovers (caused during filament winding of off-axis layers), are available.[1,2]

Fiber cross-overs are a consequence of efforts to reduce material wastage or to increase production rate in a filament winding process. Specimens can be filament wound with fiber crossovers or without fiber crossovers, as shown in Fig. 1 for cylindrical specimens. (Flat panels can be wound on a flat-sided mandrel in the same manner as shown in the figure.) As indicated in the figure, winding patterns that result in different patterns of fiber crossovers are possible. Fiber crossovers can be thought of as wavy fibers in a localized area of the specimen. These fiber crossovers cause the structural response of filament-wound specimens with fiber crossovers to differ from the structural response of filament-wound specimens without fiber crossovers and from that of specimens fabricated from hand laid-up tape, even if all specimens have the same stacking sequence. The response of filament-wound composite cylinders to tensile loading is addressed in Ref. 1, and the response of filament-wound flat sandwich plates subjected to impact damage under tensile and compressive loading is addressed in Ref. 2. Significant differences between the response of flat filament-wound and hand-laid tape specimens are presented in Ref. 2. The experimentally determined response of hand laid-up tape and filament-wound cylinders and flat panels subjected to axial compressive loading and impact damage is addressed in the present paper.

Received Feb. 4, 1991; presented as Paper 91-1080 at the AIAA/ASME/ASCE/AHS 32nd Structures, Structural Dynamics, and Materials Conference, Baltimore, MD, April 8-10, 1991; revision received June 6, 1991; accepted for publication June 20, 1991. 

*Aerospace Engineer, Aircraft Structures Branch, Structural Mechanics Division. Member AIAA.
†Engineer, Small Airplane Directorate, Atlanta Aircraft Certification Office. Member AIAA.

## Test Specimens

Seventeen panels and 27 cylinders were tested in this study. All specimens were designed to be moderately thick (with a width-to-thickness or radius-to-thickness ratio of less than 30). Panel dimensions were chosen so that the impact damage would not extend to the edges of the specimen even in the most severe case. Stacking sequences and cylinder lengths were limited by the filament-winding fabrication process. Although 0-deg plies (those oriented in the loading direction) would be desirable in many situations, such layers often cannot be filament wound. In this study, the minimum positive ply orientation possible was 30 deg. Cylinder lengths were selected because of the spacing of rows of fiber crossovers.

### Panels

Eight flat panels with a $[\pm 45/90]_{4s}$ stacking sequence were hand laid-up with Hercules Incorporated AS4 graphite fiber and 3502 thermosetting epoxy resin. These panels were nominally 25.4 cm (10 in.) long, 10.2 cm (4 in.) wide, and 0.36 cm (0.14 in.) thick. Eight flat panels with a $[\pm 30/90]_{10}$ stacking sequence were filament wound from Celanese Celion® 6K fiber and Shell Epon® 9400 toughened epoxy resin. The filament-wound graphite-epoxy flat panels were wound with 2.54-cm (1-in.)-wide tape. Four specimens were constructed using a winding pattern without fiber crossovers (also called "single circuit" pattern), and four specimens were constructed using a winding pattern with many fiber crossovers (also called "multicircuit" pattern), as shown in Figs. 1a and 1b, respectively. One hand-laid flat panel with a $[\pm 30/90]_{16}$ stacking sequence was constructed from AS4-3502 graphite-epoxy tape. These panels were nominally 25.4 cm (10 in.) long, 12.7 cm

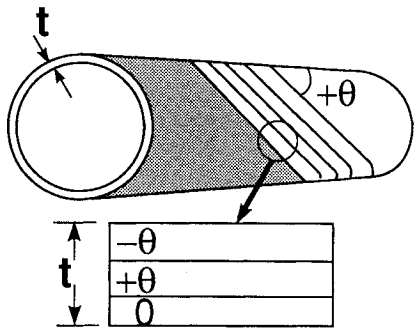


Fig. 1a Winding pattern without fiber crossovers.

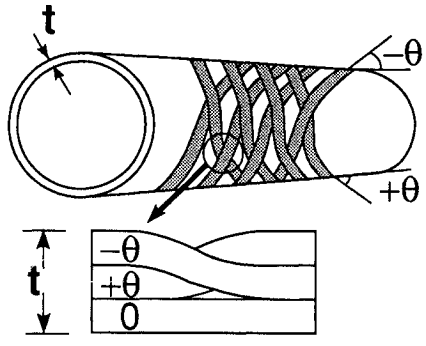


Fig. 1b Winding pattern with fiber crossovers throughout the specimen.

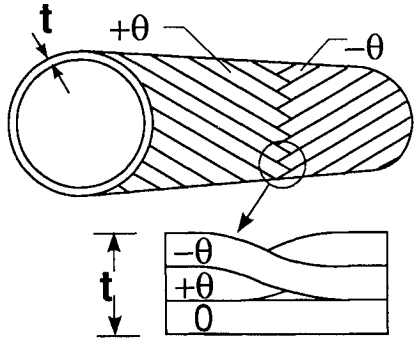


Fig. 1c Winding pattern with rows of fiber crossovers.

(5 in.) wide, and 0.64 cm (0.25 in.) thick. The dimensional parameters, materials, and manufacturing details of each nominally flat panel tested are presented in Tables 1 and 2. Both the hand-laid tape and the filament-wound unsymmetrically laminated panels had an initial bow of 6–7% of the panel thickness due to residual stresses and temperature changes in the fabrication process, despite the fact that the panels were removed from the mandrel prior to curing so there would be no tension during cure and despite a cure cycle with less than 3°C/min heating until the maximum temperature level was reached and a less than 6°C/min cool-down rate. (Identification of commercial products and companies in this report is used to describe adequately the materials. The identification of these commercial products does not constitute endorsement, expressed or implied, of such products by the National Aeronautics and Space Administration or the publishers of this journal.)

The loaded edges of all flat panels were ground flat and parallel to ensure uniform edge displacement during loading. All flat panels were instrumented with axial back-to-back strain gauges. One side of each panel was painted white so a moiré fringe technique could be used to monitor out-of-plane displacements during loading. The loaded edges of each specimen were held in a clamping fixture during testing, and the unloaded edges were supported with knife edges. Photographs showing the winding pattern of a typical filament-wound flat panel with many fiber crossovers and the comparable tape panel (with no fiber crossovers) are shown in Fig. 2. The panels shown in Fig. 2 were tested in compression to failure, and their failures modes are discussed in a subsequent section.

Table 1 Stacking sequences and fabrication method

| Designation | Stacking sequence | Material | Fabrication method[a] |
|---|---|---|---|
| | Panels | | |
| A | $[\pm 45/90]_{4s}$ | AS4-3502 | tape |
| B | $[\pm 30/90]_{16}$ | AS4-3502 | tape |
| C | $[\pm 30/90]_{10}$ | Celion 6K-9400 | fw |
| | Cylinders | | |
| D | $[\pm 45/90]_{3s}$ | AS4-3502 | fw |
| E | $[\pm 30/90]_{2}$ | AS4-Ryton | fw |
| F | $[\pm 30/90]_{7}$ | AS4-Ryton | fw |
| G | $[\pm 45/90]_{3s}$ | AS4-3502 | tape |

[a]fw represents filament wound; tape represents hand-laid tape.

Table 2 Flat panels tested

| Specimen type[a] | Fiber crossovers | Impact energy, J (ft-lb) | $w/t$[b] | $\delta/L$,[c] % |
|---|---|---|---|---|
| A | No | 0 | 30.5 | 1.28 |
| | No | 1.47 (1.07) | 30.2 | 1.28 |
| | No | 3.38 (2.47) | 30.6 | 1.05 |
| | No | 4.33 (3.17) | 30.7 | 0.75 |
| | No | 5.97 (4.38) | 30.6 | 0.63 |
| | No | 8.48 (6.21) | 30.6 | 0.55 |
| | No | 10.4 (7.64) | 30.7 | 0.58 |
| | No | 12.2 (8.98) | 30.6 | 0.47 |
| B | No | 0 | 18.8 | 0.95 |
| C | Yes | 0 | 20.8 | 0.95 |
| | Yes | 12.6 (9.21) | 20.9 | 0.53 |
| | Yes | 22.0 (16.1) | 20.5 | 0.40 |
| | Yes | 35.0 (25.6) | 20.9 | 0.34 |
| | No | 0 | 17.5 | 1.09 |
| | No | 12.6 (9.21) | 18.6 | 0.75 |
| | No | 22.2 (16.3) | 17.5 | 0.54 |
| | No | 34.5 (25.3) | 18.7 | 0.40 |

[a]See Table 1 for stacking sequence.
[b]$w$ is panel width; $t$ is panel thickness; all panels were 25.4 cm long.
[c]$\delta$ is the end-shortening; $L$ is the panel length.

### Cylinders

Eight graphite-thermoplastic filament-wound, 8 graphite-epoxy filament-wound, and 11 graphite-epoxy hand laid-up tape cylinders were tested. All graphite-epoxy cylinders were fabricated from Hercules Incorporated AS4 graphite fiber and 3502 thermosetting epoxy resin. All graphite-thermoplastic cylinders were fabricated from Hercules Incorporated AS4 fiber and Phillips Petroleum Ryton® thermoplastic resin. The dimensions, materials, and manufacturing details of each cylinder tested are presented in Tables 1 and 3.

All graphite-epoxy cylinders had a $[\pm 45/90]_{3s}$ stacking sequence. Four graphite-epoxy cylinders had no fiber crossovers in the test section, and four had fiber crossovers located in the center of the test section. These winding patterns are shown in Figs. 1a and 1c, respectively. A photograph of a cylinder with fiber crossovers is shown in Fig. 3. The graphite-epoxy filament-wound cylinders were wound with 1.27-cm (0.5-in.)-wide tape. Filament-wound and hand-laid tape graphite-epoxy cylinders had an inner radius of 3.18 cm (1.25

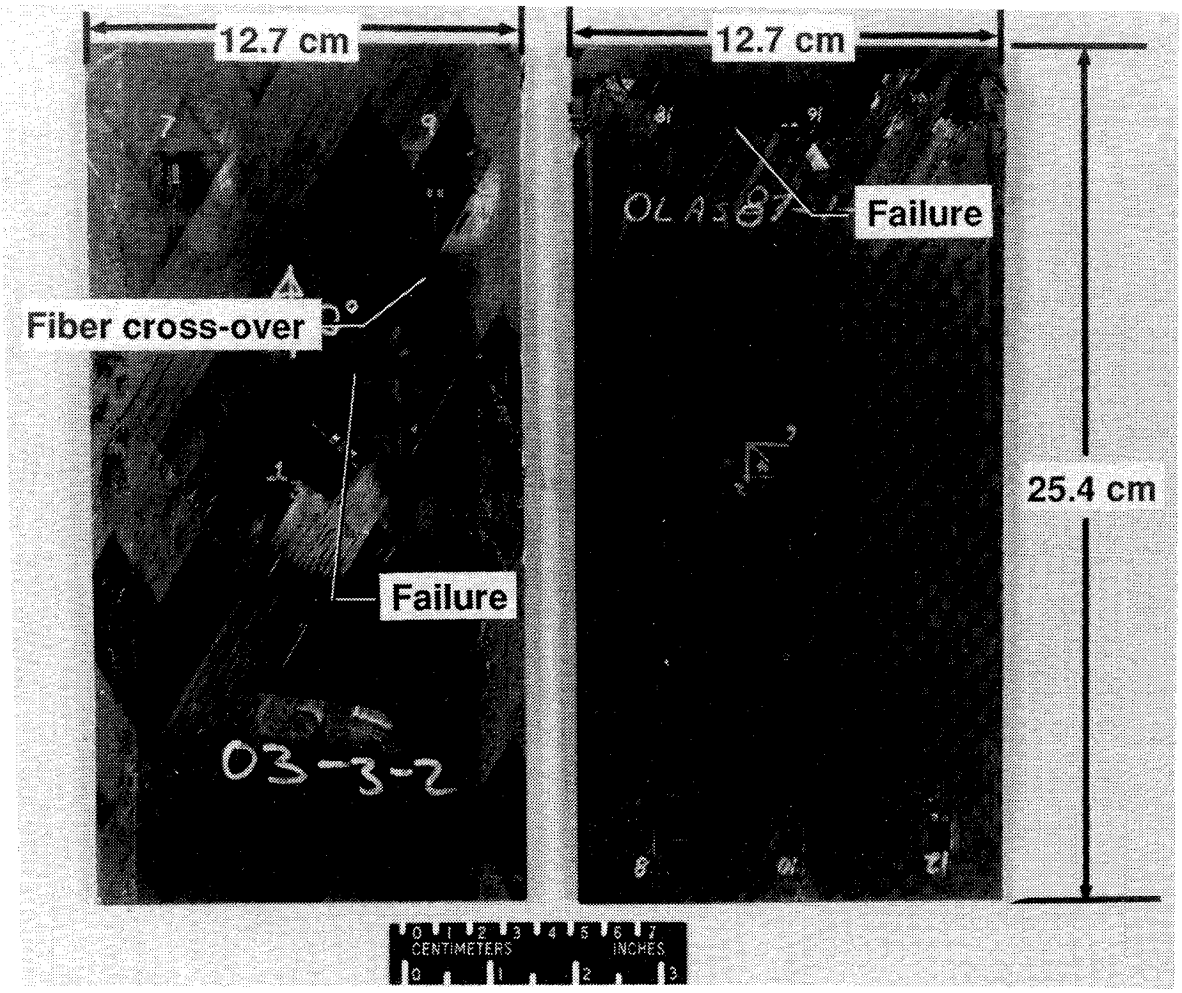


Fig. 2 Filament-wound and hand-laid tape flat panels.

Table 3 Cylinders tested

| Specimen type[a] | Fiber crossovers | Impact energy, J (ft-lb) | $R/t$[b] | $\delta/L$,[c] % |
|---|---|---|---|---|
| D | No | 0 | 8.93 | 2.09 |
| | No | 0 | 8.33 | 2.09 |
| | No | 1.38 (1.01) | 8.93 | 1.61 |
| | No | 5.09 (4.31) | 8.33 | 0.95 |
| | Yes | 0 | 12.50 | 1.82 |
| | Yes | 0 | 8.86 | 1.88 |
| | Yes | 0 | 8.33 | 2.18 |
| | Yes | 4.81 (3.52) | 8.33 | 1.02 |
| E | Yes | 0 | 29.2 | 0.39 |
| | Yes | 0.34 (0.25) | 28.8 | 0.57 |
| | Yes | 1.38 (1.01) | 29.2 | 0.49 |
| | Yes | 5.58 (4.09) | 30.5 | 0.46 |
| F | Yes | 0 | 10.0 | 0.51 |
| | Yes | 0.81 (0.59) | 9.0 | 0.48 |
| | Yes | 4.11 (3.01) | 10.0 | 0.64 |
| | Yes | 12.50 (9.13) | 8.9 | 0.29 |
| G | No | 0 | 10.3 | 1.60 |
| | No | 0 | 10.4 | 1.99 |
| | No | 0 | 12.5 | 1.57 |
| | No | 0 | 10.2 | 2.23 |
| | No | 0 | 10.4 | 2.23 |
| | No | 0 | 10.0 | 1.84 |
| | No | 0 | 10.0 | NA |
| | No | 1.31 (0.96) | 11.4 | 1.40 |
| | No | 5.50 (4.03) | 10.4 | 0.83 |
| | No | 10.20 (7.47) | 11.4 | 0.75 |
| | No | 20.60 (15.1) | 12.5 | 0.68 |

[a]See Table 1 for stacking sequence.
[b]$R$ is cylinder inner radius; $t$ is cylinder wall thickness.
[c]$\delta$ is the end-shortening; $L$ is the panel length.

in.) and a nominal skin thickness of 0.36 cm (0.14 in.) and were cut to a nominal length of 15.3 cm (6 in.).

Four graphite-thermoplastic cylinders were wound with a $[\pm 30/90]_7$ stacking sequence and a nominal wall thickness of 0.35 cm (0.138 in.), and four cylinders were wound with a $[\pm 30/90]_2$ stacking sequence and a nominal wall thickness of 0.12 cm (0.048 in.). All graphite-thermoplastic cylinders were nominally 20.3 cm (8 in.) long with an inner radius of 3.52 cm (1.385 in.). The graphite-thermoplastic cylinders were wound with 0.63-cm (0.25-in.)-wide tape and had fiber crossovers at axial locations 6.4 cm (2.5 in.) apart.

Before testing, 1 in. on each end of each cylindrical specimen was plotted in an epoxy compound to simulate clamped boundary conditions. The ends were ground flat and parallel to ensure uniform end displacement during loading. All cylinders were instrumented with back-to-back strain gauge rosettes on the interior and exterior surfaces. One side of each cylinder was painted white so a moiré fringe technique could be used to monitor out-of-plane displacements during loading. A photograph of a graphite-epoxy tape cylinder before testing is shown in Fig. 3.

## Apparatus and Tests

All specimens were loaded in axial compression in a hydraulic testing machine. The load was applied slowly to simulate static conditions. Load rates of 35–45 kN/min (8000–10,000 lb/min) for the thickest specimens and 11 kN/min (2400 lb/min) for the thinner specimens were used. All specimens except one graphite-epoxy tape cylinder were loaded to failure. Load, strain, out-of-plane displacements, and end-shortening data were recorded during each test. Out-of-plane displacement patterns (moiré fringe patterns) were photographed dur-

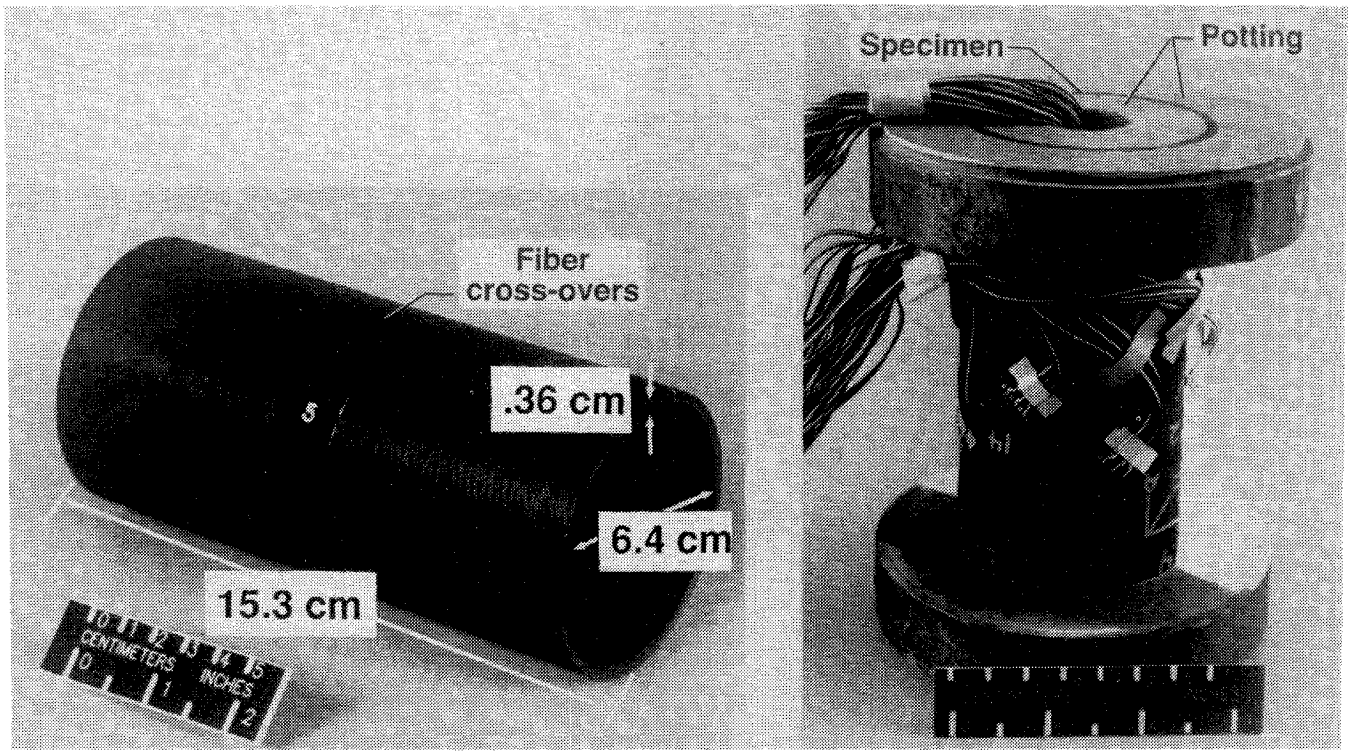


Fig. 3 Graphite-epoxy cylinders before testing.

ing each test. Many specimens were impact-damaged before compressive loading. The specimens were impacted using a 1.27-cm (0.5-in.)-diameter aluminum sphere propelled at a specified speed using the impacting system described in Ref. 3. Cylinders were impacted midlength, and flat panels were impacted at the center of the test section. Impact energy for each of the panels and each cylinder specimen is shown in Tables 2 and 3, respectively.

## Results and Discussion

Test results for four types of specimens are presented in this section. Comparisons are made between filament-wound flat panels with and without fiber crossovers, undamaged filament-wound and hand laid-up tape graphite-epoxy cylinders, impact-damaged graphite-epoxy cylinders and flat panels, and graphite-thermoplastic cylinders with and without impact damage.

### Graphite-Epoxy Specimens

#### $[\pm 30/90]_n$-Class Panels

Eight graphite-epoxy filament-wound flat panels with a $[\pm 30/90]_{10}$ stacking sequence and one hand-laid tape panel with a $[\pm 30/90]_{16}$ stacking sequence, as described in Tables 1 and 2, were tested. Data for similar graphite-epoxy panels made from hand-laid tape and containing cutouts are presented in Ref. 4.

The normalized load $P/EA$ (where $P$ is the applied load, $E$ is the experimentally determined specimen effective axial modulus, and $A$ is the specimen initial cross-sectional area) vs the normalized displacement $\delta/L$ (where $\delta$ is the end shortening and $L$ is the specimen initial length) for three control (undamaged) panels is shown in Fig. 4. The control panel with fiber crossovers and the tape panel failed at a load and end-shortening about 20% below that of the filament-wound control panel without fiber crossovers. The tape control panel failed near a clamped edge, whereas both the filament-wound control panel with fiber crossovers and the filament-wound control panel without fiber crossovers failed across the axial center of the specimen. The filament-wound control panel with many fiber crossovers and the tape panel are shown in

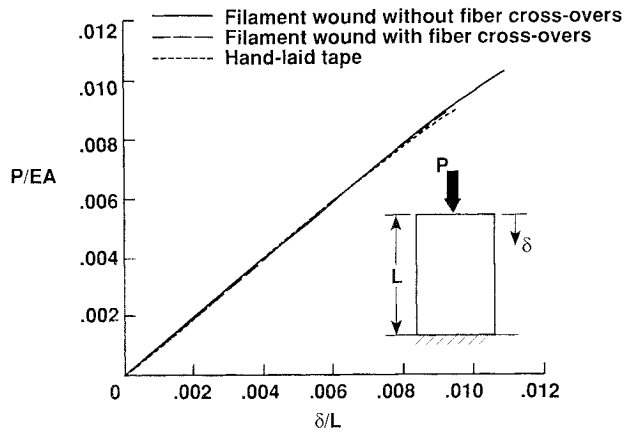


Fig. 4 Normalized load-shortening relationship of graphite-epoxy control flat panels with a $[\pm 30/90]_n$ stacking sequence (where $n = 10$ or 16).

Fig. 2. The experimentally determined effective axial modulus of the filament-wound control panels with and without fiber crossovers are 20% and 31%, respectively, less than that of the tape control panel. However, because of differences in thickness, the experimentally determined stiffness $EA$ of the filament-wound panels is about 28% less than that of the tape panel. The average modulus and stiffness for each type of specimen are shown in Table 1.

Axial surface strains determined from back-to-back strain gauges in the center of the three control panels are shown in Fig. 5. The strains are shown on the abscissa, and the normalized load $P/EA$ is shown on the ordinate. The strain gauges recorded a linear load-strain relationship almost to failure in each case. All control panels buckled at loads within 10% of failure load. The response of the three control panels was the same for both the filament-wound and tape specimens at low strain levels.

The remaining six panels were impacted with impact energies ranging from 12 to 35 J (9 to 26 ft-lb) corresponding to

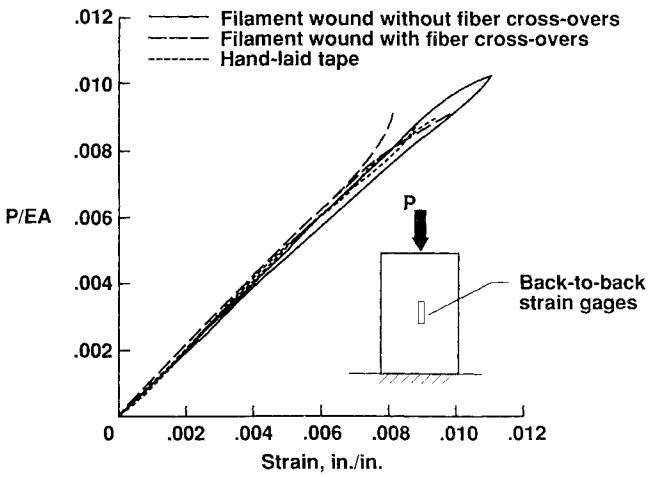


Fig. 5 Axial surface strain in the center of graphite-epoxy control flat panels with a $[\pm 30/90]_n$ stacking sequence (where $n = 10$ or 16).

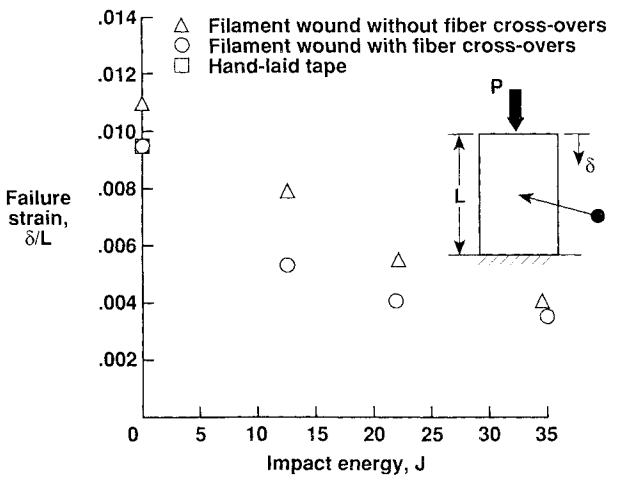


Fig. 6 Effect of impact damage on failure strain of graphite-epoxy flat panels with a $[\pm 30/90]_n$ stacking sequence (where $n = 10$ or 16).

impact speeds of 91 to 153 m/s (300 to 500 ft/s) before compressive loading. All impact-damaged specimens failed through the impact site (center of the panel) and did not buckle prior to failure. Failure strains ($\delta/L$ at failure) for control and impact-damaged specimens of each type are presented in Table 2 and shown in Fig. 6. All impact-damaged specimens exhibited significant reduction in failure strains when compared to the control panels. For all impact energy levels considered, the specimen with fiber crossovers exhibited a lower failure strain than the specimen without fiber crossovers. The effect of fiber crossovers was to reduce the failure strain by 5–30% in this study.

*$[\pm 45/90]_{3s}$ Cylinders*

Five graphite-epoxy filament-wound control cylinders, as described in Tables 1 and 3, were loaded in axial compression to failure. The failure strain ($\delta/L$ at failure) of each specimen is shown in Fig. 7 and given in Table 3. The horizontal bars in the figure represent the average failure strain of cylinders of each type, and the symbols represent the failure strain of each cylinder. Average failure strains of the two types of filament-wound control cylinders differ by less than 10%, which is within the scatter range of the results, indicating that the presence of fiber crossovers has little effect on failure strain.

Six tape control cylinders were loaded to failure in axial compression. The failure strain ($\delta/L$ at failure) of each cylinder is shown in Fig. 7 and given in Table 3. The horizontal bar in the figure represents the average failure strain of the tape cylinders, and the symbols represent the failure strain of each cylinder. A larger scatter range is evident for the tape cylinders than for the filament-wound cylinders. The average failure strain of the tape cylinders is approximately 10% lower than the average failure strain of the filament-wound cylinders (including those with and without fiber crossovers). However, with such a large scatter range, for a larger population of specimens, it is expected that there may be no significant difference in failure strains between tape and filament-wound cylinders. Fiber weight fractions for pieces cut from failed cylinders were determined via an acid digestion technique. The variation in fiber weight fraction among tape cylinders, filament-wound cylinders away from fiber crossovers, and filament-wound cylinders at fiber crossovers was less than 2%.

The normalized load $P/EA$ vs the normalized displacement $\delta/L$ for a typical filament-wound and a typical tape cylinder is shown in Fig. 8. The effective axial modulus, calculated from experimental data from each cylinder in the linear-elastic range, indicates that the effective modulus of the tape cylinders is 12% higher than that of the filament-wound cylinders, as shown in Table 1. However, the average thickness

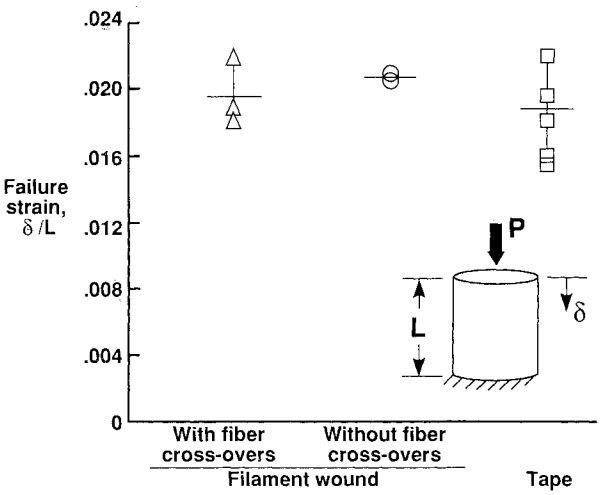


Fig. 7 Average failure strain of graphite-epoxy control cylinders with a $[\pm 45/90]_{3s}$ stacking sequence.

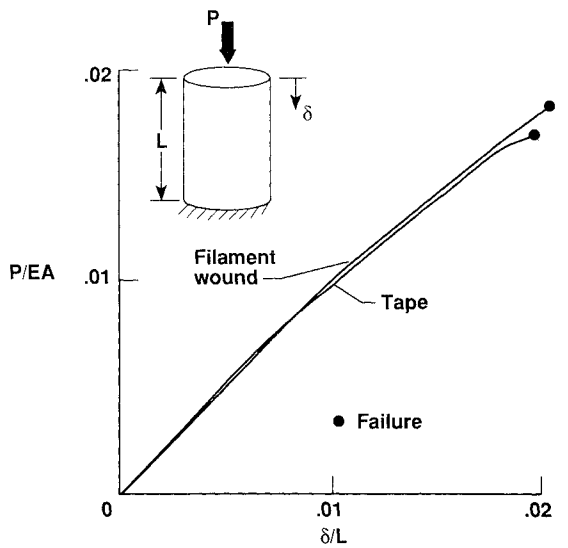


Fig. 8 Normalized load-displacement relationship of typical filament-wound and tape graphite-epoxy control cylinders with a $[\pm 45/90]_{3s}$ stacking sequence.

of the filament-wound cylinders (based on four measurements on each end of each cylinder) is 15% higher than that of the tape cylinders. The average stiffness $EA$ for the filament-wound cylinders is approximately 10% higher than the average $EA$ for the tape cylinders. In both types of cylinders, the scatter of values for $EA$ among the cylinders tested is about 8% whereas the scatter for $E$ is about 20%. The load-displacement relationship is nonlinear in both types of cylinders when the axial strain is greater than about 0.01 and results in a decrease in axial stiffness. As indicated by the data shown in the figure, the cylinders respond similarly in the linear-elastic range, with the tape cylinder curve slightly above that of the filament-wound cylinder; however, the curves cross at a $\delta/L$ of approximately 0.008, resulting in the curve representing the filament-wound cylinder being above that of the tape cylinder until failure.

Back-to-back axial surface strain measurements recorded at midlength of two typical specimens are shown in Fig. 9. The strains are shown on the abscissa, and the normalized load $P/EA$ is shown on the ordinate. Solid lines represent strains measured by interior gauges, and dashed lines represent strains measured by exterior gauges. Little difference in behavior is seen among the four gauges (interior and exterior measurements from tape and filament-wound cylinders). There is no discontinuity in slope or significant difference between strains recorded by back-to-back gauges in the filament-wound or tape cylinders. None of the cylinders tested exhibited buckling behavior or local out-of-plane displacements before failure. All graphite-epoxy specimens failed in a similar manner. Photographs of a failed tape specimen are shown in Fig. 10. The failure mode involved the innermost and outermost plies at the midlength of the specimen failing and delaminating from the adjoining plies. Little visible or audible warning occurred before failure. Failure quickly progressed around the circumference of the cylinder. Axial surface strains measured at midlength were lightly over 0.02 at failure in each specimen. Gauges in the direction of the outermost fibers (45 deg) recorded failure strains in the range of 0.007–0.008.

One tape cylinder was loaded to approximately 90% of the failure load. Acoustic emission measurements were used to determine when to stop loading. The specimen was then unloaded so that initial internal damage could be examined. No visible exterior damage was evident. The potting material and strain gauge wires were removed, and the specimen was subjected to ultrasonic examination. This examination revealed that a 2-in.-square area near the potting material had suffered interior damage where no damage was visible on the inner or outer surface. Strips were cut from the damaged region for microscopic examination. This examination revealed that delamination between plies had occurred near the outer surface. There was little evidence of fiber breakage.

Before loading, three filament-wound and four tape graphite-epoxy cylinders were impacted at impact speeds up to 122 m/s (400 ft/s), corresponding to impact energies up to 22.2 J (16 ft-lb). The failure strain of each impacted specimen and

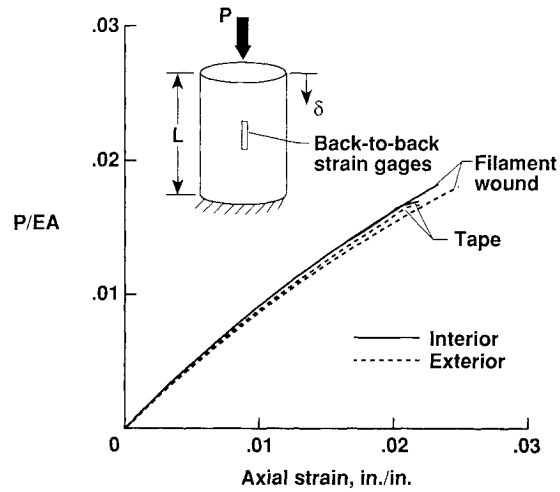


**Fig. 9 Typical axial surface strain of filament-wound and tape cylinders with a $[45/90]_{3s}$ stacking sequence.**

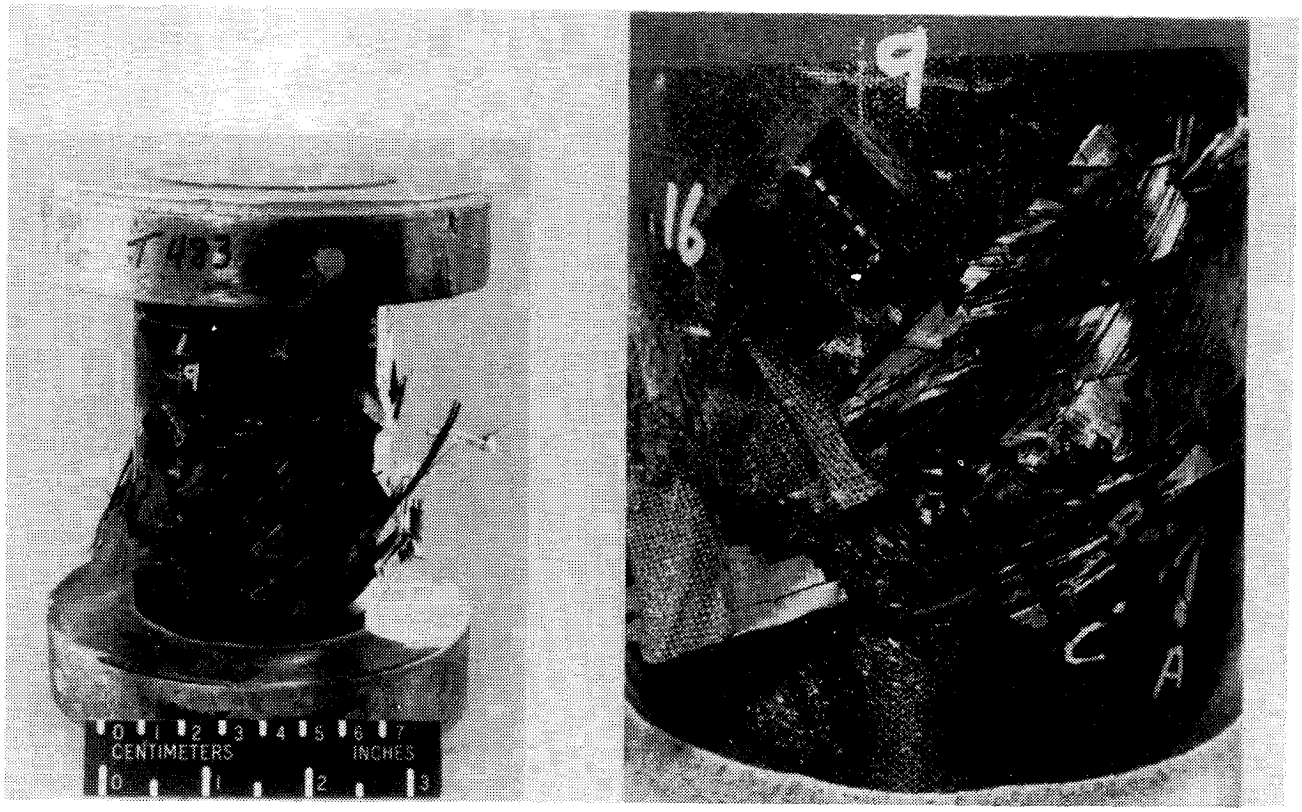


**Fig. 10 Failed graphite-epoxy tape cylinder.**

the average failure strain of all control specimens of each type are shown in Fig. 11 as a function of impact energy. The circles and squares in the figure represent filament-wound and tape cylinders, respectively. These results indicate that impact damage reduces the failure strain to approximately 60% of the average failure strain of unimpacted specimens for impact energies over 5.5 J (4 ft-lb) for filament-wound and tape cylinders. The minimum failure strain for impacted cylinders is approximately 0.006. Failure modes for impacted cylinders were the same as for unimpacted cylinders. Impacted specimens failed through the impact site (midlength).

*$[\pm 45/90]_{4s}$ Flat Panels*

Eight flat graphite-epoxy panels were also tested. These specimens had the same nominal thickness as the graphite-epoxy cylinders. The control panel buckled into three half-waves at a $\delta/L$ of approximately 0.011 (prior to failure) and then failed at a nodal line at an axial strain lower than that of the cylinders. Experimentally determined prebuckling stiffness $EA$ of the control panel is about half the initial stiffness $EA$ of the tape cylinders. The remaining seven flat graphite-epoxy panels were subjected to low-speed impact damage before compressive loading. The specimen impacted with 1.47 J buckled and failed in the same manner as the control panel. All other specimens did not buckle before failure and failed through the impact site. Failure strains of the impact-damaged flat specimens are presented in Table 2 and are shown in Fig. 11. The flat panels failed at lower strains than did the cylinders for each impact energy. Among specimens impacted at impact energies above 5.5 J (4 ft-lb), the flat panels have a lower initial extensional stiffness than the cylinders and they fail at a lower strain. The minimum failure strain for flat panels is approximately 0.0045. A similar series of tests of flat panels with a similar stacking sequence but twice the thickness resulted in a minimum failure strain of 0.0044, as described in Ref. 5.

**Graphite-Thermoplastic Cylinders**

Four thicker-walled (radius-to-thickness ratio approximately 10) and four thinner-walled (radius-to-thickness ratio approximately 30) graphite-thermoplastic filament-wound cylinders were tested. Each specimen contained many fiber crossovers. One control specimen of each thickness was loaded in axial compression to failure. Typical interior and exterior axial surface strains of the thicker control cylinder are shown in Fig. 12a. The strain gauge measurements are shown on the abscissa, and a normalized load $P/EA$ is shown on the ordinate. Significant differences can be seen in the recorded strains of back-to-back strain gauges, although each gauge records a linear load-strain relationship. Control specimens failed in a thin line around the circumference of the cylinder at an axial location where a line of fiber crossovers occurs on the interior of the specimen. Damage did not spread to other parts of the cylinder. The exterior 90-deg ply on the graphite-thermoplastic cylinders did not have the wavy fibers characteristic of fiber crossovers and had significantly lower stresses than the interior ±30-deg layer.

A linear finite element analysis of the thicker control cylinder using the computer code STAGS[6] and the graphite-thermoplastic properties presented in Table 4 is used to examine the stress state in the inner and outer plies of the cylinder. The normalized axial stress distribution along the length of the cylinder predicted by the analysis, represented by solid lines, is shown in Fig. 12b. Analysis indicates that boundary effects are limited to within about 2.54 cm from the clamped edge. Experimental results of calculated stress based on strain gauge measurements recorded at four points around the circumference of the cylinder 2.5 cm away from midlength and four points 3.5 cm away from midlength, represented by open symbols, are also shown in Fig. 12b. These gauges were 2.0 and 3.2 cm from the nearest fiber crossovers. In a perfect cylinder subjected to purely axisymmetric load, the circumferential position would be irrelevent and all strain gauge data points from one axial location on a given surface would lie one on top the other. No variation around the circumference is seen in the analytical results. In the test data shown in the figure, significant variation is seen in data recorded at the same axial but different circumferential locations. Two factors contribute to the difference between the strain recorded at different points around the circumference and the difference between interior and exterior recorded strains. First, the strain gauges were located near the fiber crossovers. The proximity of the strain gauges to the fiber crossovers probably caused variation in measurements among the interior gauges. Fiber crossovers were not included in the analysis. Second, the interior ply is a wound ±30-deg layer and the exterior ply is a 90-deg layer. The measured strains (and calculated stresses shown in Fig. 12b) are therefore not the same on the interior and the exterior of the cylinder. The stress analysis also indicates this difference, as shown by the two solid lines in Fig. 12b. Little difference between interior and exterior measurements would be seen in a symmetrically laminated specimen

**Table 4 Graphite-thermoplastic material properties**

| | |
|---|---|
| Longitudinal Young's modulus, $E_1$ | 133.8 GPa |
| Transverse Young's modulus, $E_2$ | 8.9 GPa |
| Shear modulus, $G_{12}$ | 5.1 GPa |
| Major Poisson's ratio, $\mu_{12}$ | 0.38 |

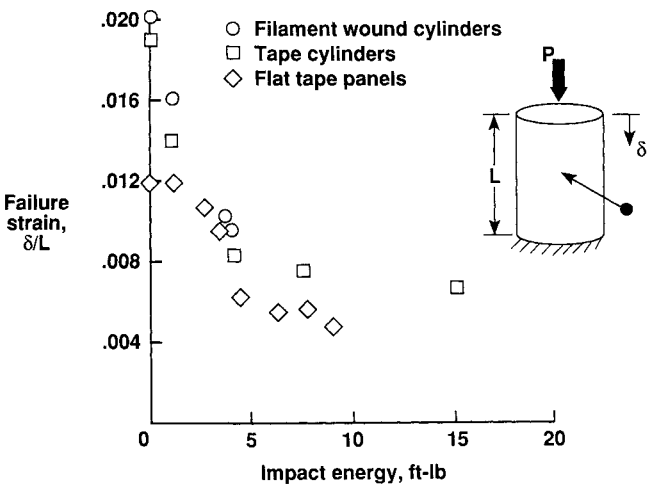


**Fig. 11 Effect of impact damage on failure strain of graphite-epoxy cylinders and flat panels with a $[\pm 45/90]_{ns}$ stacking sequence (where $n$ = 3 or 4).**

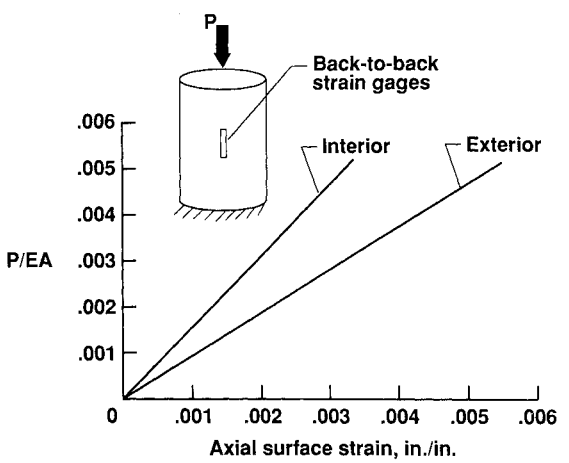


**Fig. 12a Typical axial surface strains of a thick-walled graphite-thermoplastic control cylinder with a $[\pm 30/90]_7$ stacking sequence.**

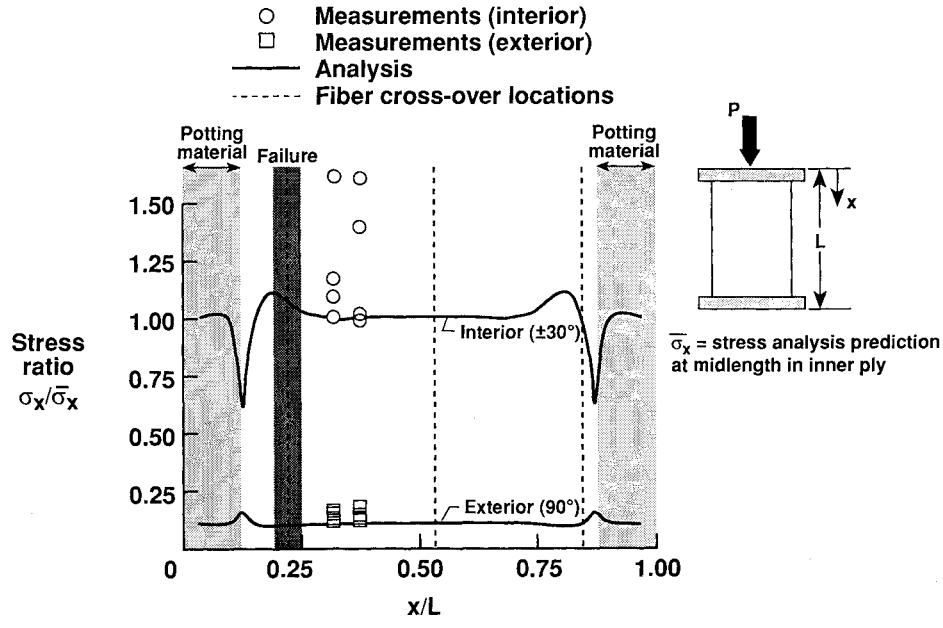


Fig. 12b Normalized stress distribution in outermost and innermost layers of graphite-thermoplastic control cylinder with a $[\pm 30/90]_7$ stacking sequence based on analysis and strain gauges.

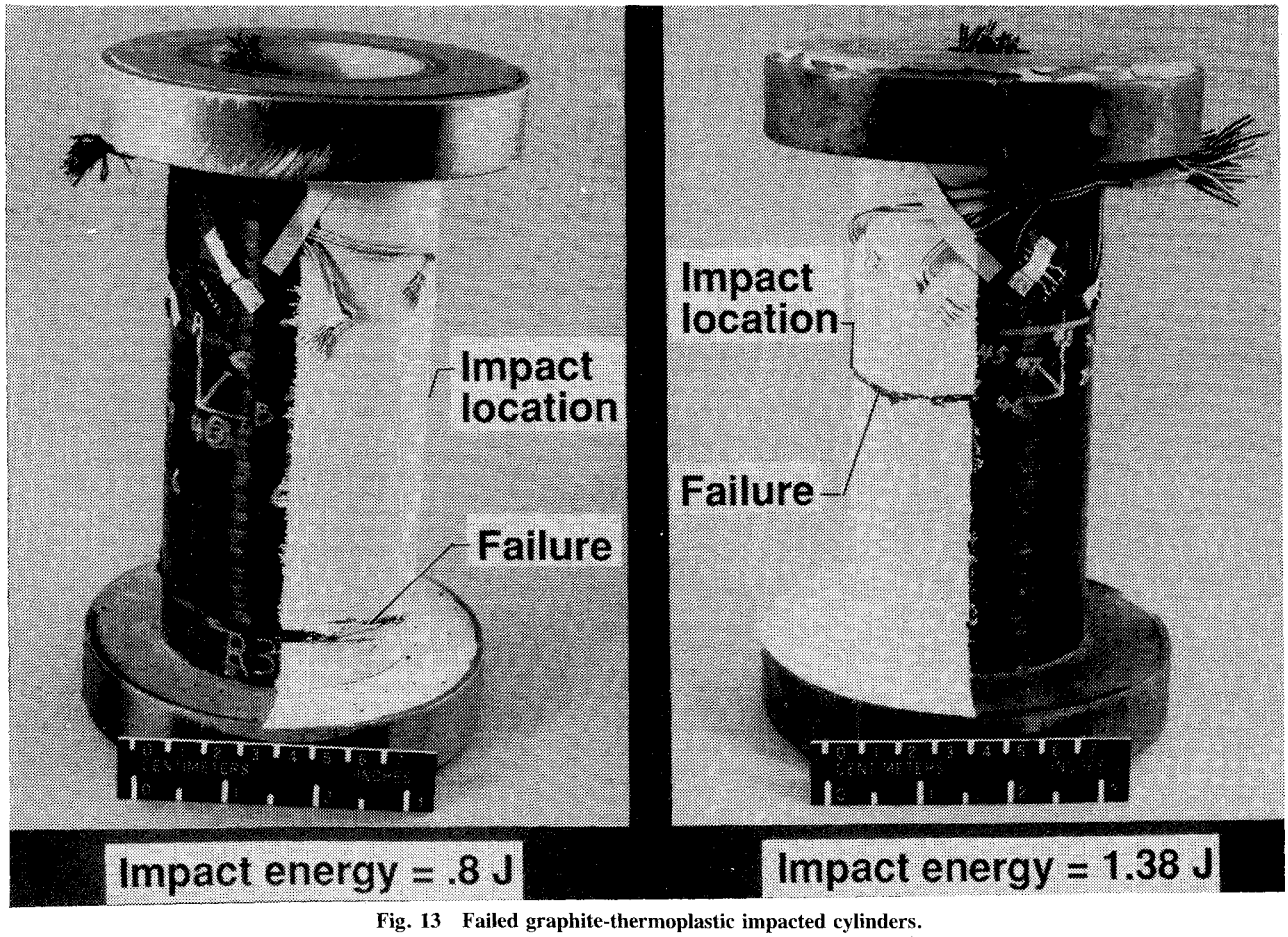


Fig. 13 Failed graphite-thermoplastic impacted cylinders.

(such as the graphite-epoxy cylinders previously discussed).

The other cylinders were impacted at energies varying from 0.34 to 12.5 J (0.25 to 9.2 ft-lb) before compressive loading. The graphite-thermoplastic cylinders subjected to impact energies of less than 1.1 J (0.82 ft-lb) failed at an interior fiber crossover location, as in the control specimens. The specimens impacted at energies greater than 1.1 J failed through the impact location and all around the circumference, although not at an interior fiber crossover location. Photographs showing exterior damage after failure are presented in Fig. 13. The failure location is evident on the painted side of the cylinders.

Failure strain ($\delta/L$ at failure) of control and impacted specimens are presented in Table 3 and shown in Fig. 14 for all graphite-thermoplastic specimens tested. Comparison of failure strains for each specimen seems to indicate that the failure

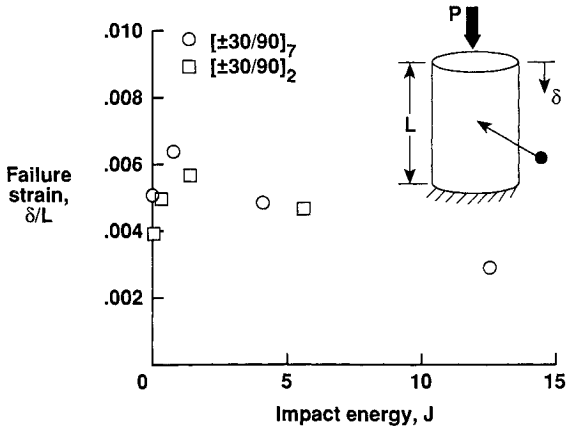


**Fig. 14 Effect of impact damage on failure strain of graphite-thermoplastic filament-wound cylinders.**

strain of the thin cylinder impacted with an impact energy of 1.38 J (1. ft-lb) and the failure strain of the thick cylinder impacted with 4.11 J (3. ft-lb) are higher by 30% and 18%, respectively, than the failure strains of the corresponding undamaged cylinders. Impacts at higher energy levels slightly reduce failure strain. Similar results are obtained by comparing failure load as a function of impact energy. Impacts at higher energies than considered here would be needed to establish a minimum failure strain threshold.

## Concluding Remarks

A comparison of experimental results for filament-wound graphite-epoxy panels with a $[\pm 30/90]_{10}$ stacking sequence constructed with two different winding patterns and loaded in axial compression indicates that unimpacted filament-wound panels with many fiber crossovers fail at up to 15% lower strains than do filament-wound panels without fiber crossovers. However, a comparison of undamaged filament-wound graphite-epoxy cylinders loaded to failure in axial compression indicates that one fiber crossover location has no effect on the failure mode or failure strain of thick-walled filament-wound graphite-epoxy specimens with a $[\pm 45/90]_{3s}$ stacking sequence. A comparison between filament-wound and hand laid-up tape undamaged cylinders indicates that there is little or no difference in the average failure strain of cylinders constructed by using the two different fabrication methods, and all cylinders demonstrated the same failure mode. However, the variation of failure strain is more significant for the tape cylinders than for the filament-wound cylinders.

A comparison of specimens subjected to low-speed impact damage before compressive loading indicates that impact damage reduces the strain at failure by over 60% in tape flat panels and in tape and filament-wound graphite-epoxy cylinders with a $[\pm 45/90]_{ns}$ stacking sequence. The presence of fiber crossovers reduced the failure strain of filament-wound impact-damaged panels for all impact energies considered. The failure strain of the filament-wound graphite-thermoplastic cylinders studied was not reduced by low-speed impact damage. Graphite-epoxy and graphite-thermoplastic cylinders demonstrated significantly different failure modes. The graphite-epoxy specimens failed over approximately one third of the specimen, whereas the graphite-thermoplastic cylinders failed in a thin line around the circumference of the cylinder.

## References

[1]Floral, R. F., and Gilbreath, D. R., "Delamination Failure Modes in Filament-Wound Composite Tubes," *Composite Materials: Fatigue and Fracture*, Vol. 2, ASTM STP 1012, 1989, pp. 313–325.

[2]Llorente, S. G., and Mar, J. W., "The Residual Strength of Filament Wound Graphite/Epoxy Sandwich Laminates Due to Impact Damage and Environmental Conditioning," AIAA Paper 89-1275-CP, Mobile, AL, April 1989.

[3]Starnes, J. H., Jr., Rhodes, M. D., and Williams, J. G., "Effect of Impact Damage and Holes on the Compression Strength of a Graphite/Epoxy Laminate," *Nondestructive Evaluation and Flaw Criticality for Composite Materials*, ASTM STP 696, 1979, pp. 145–171.

[4]Rhodes, M. D., Mikulas, M. M., Jr., and McGowan, P. E., "Effects of Orthotropy and Width on the Compression Strength of Graphite-Epoxy Panels with Holes," *AIAA Journal*, Vol. 22, No. 9, 1984, pp. 1283–1292.

[5]Shuart, M. J., and Williams, J. G., "Compression Behavior of ±45°-Dominated Laminates with a Circular Hole or Impact Damage," *AIAA Journal*, Vol. 24, No. 1, 1986, pp. 115–122.

[6]Almroth, B. O., and Brogan, F. A., "The STAGS Computer Code," NASA CR-2950, 1980.